Applied Physics Letters

RESEARCH ARTICLE | APRIL 15 2021

Broadband waveguide-integrated superconducting single-photon detectors with high system detection efficiency

Martin A. Wolff; Fabian Beutel; Jonas Schütte; ... et. al

Appl. Phys. Lett. 118, 154004 (2021)
https://doi.org/10.1063/5.0046057

AIP Publishing

Applied Physics Letters ARTICLE scitation.org/journal/apl

Broadband waveguide-integrated superconducting single-photon detectors with high system detection efficiency

Cite as: Appl. Phys. Lett. **118**, 154004 (2021); doi: 10.1063/5.0046057
Submitted: 31 January 2021 · Accepted: 29 March 2021 ·
Published Online: 15 April 2021 · Publisher error corrected: 19 April 2021

View Online Export Citation CrossMark

Martin A. Wolff,[1,2,3] Fabian Beutel,[1,2,3] Jonas Schütte,[1,2,3] Helge Gehring,[1,2,3] Matthias Häußler,[1,2,3] Wolfram Pernice,[1,2,3] and Carsten Schuck[1,2,3,a)]

AFFILIATIONS

[1]Institute of Physics, University of Münster, Wilhelm-Klemm-Str. 10, 48149 Münster, Germany
[2]CeNTech–Center for Nanotechnology, Heisenbergstr. 11, 48149 Münster, Germany
[3]SoN–Center for Soft Nanoscience, Busso-Peus-Straße 10, 48149 Münster, Germany

Note: This paper is part of the APL Special Collection on Non-Classical Light Emitters and Single-Photon Detectors.
[a)]**Author to whom correspondence should be addressed:** carsten.schuck@uni-muenster.de

ABSTRACT

Fast and efficient detection of single photons with high timing accuracy is a crucial requirement in most quantum optics experiments and enables novel sensing and imaging solutions. Superconducting nanowire single-photon detectors (SNSPD) achieve technology-leading performance in terms of detection efficiency, dark count rate, timing jitter, and detector dead times. However, conventional SNSPDs with high system detection efficiency typically rely on resonant enhancement of the absorption efficiency, thus only achieving attractive detector benchmarks over narrow spectral windows. Waveguide-integrated SNSPDs allow for leveraging the wideband material absorption in superconducting nanowires by absorbing light in a traveling-wave geometry but have been limited to low system detection efficiencies due to interface losses when coupling to optical fibers. Here, we show how high system detection efficiencies of 22%–73% are realized over a broad wavelength range from 532 nm to 1640 nm in a single waveguide-integrated SNSPD device. We accomplish efficient coupling between optical fibers and waveguide-integrated nanowire detectors by employing a 3D interface, produced in direct laser writing, that relies on total internal reflection for achieving a broad transmission bandwidth. We further find low timing jitter of 25.7 ps and detector decay times of 9.8 ns, allowing for single-photon counting with high repetition rates up to 100 MHz. Our work paves the way for an efficient single-photon detector solution that combines the spectral requirements of an extremely wide range of quantum optics experiments in a single device. The coupling approach and SNSPD-integration with nanophotonic circuits are further well-suited for realizing large-scale detector arrays.

Experiments in quantum optics, remote sensing, and ranging, as well as lifetime-based imaging techniques all rely to a large extent on the detection of single photons over a wide range of wavelengths, from the visible into the infrared part of the spectrum, with high detection efficiency, low dark count rates, and accurate timing. This is particularly important for practical implementations of quantum technology, exhibiting some of the most stringent performance requirements, as it is obvious in quantum communication scenarios,[1] quantum sensing,[2] and quantum information processing.[3] However, no single-photon detector technology currently delivers consistent performance over a broad spectral range in a single device. Photomultiplier tubes, silicon avalanche photo diodes (APD), and indium gallium arsenide APDs only cover a limited spectral range and, in some cases, suffer from low efficiency, long dead times, timing inaccuracies, high dark count rates, and other artifacts, such as afterpulsing.[4]

Superconducting nanowire single-photon detectors (SNSPDs) offer performance improvements across all relevant benchmarks, and their material absorption remains high from the ultra-violet into the mid-infrared spectral regions. In conventional SNSPDs, detection efficiencies up to 98% were recently demonstrated at 1550 nm wavelength.[5] In order to achieve high absorption efficiencies in the few-nm thin superconducting nanowires under normal incidence from an optical fiber, however, distributed Bragg-reflectors (DBRs) and Au-reflector-based resonant structures are typically used.[5–7] Such structures can be challenging to fabricate and generally impose bandwidth restrictions, thus limiting the wavelength range over which attractive detector performance is realized to relatively small spectral windows, typically tailored to one particular application of interest, e.g., the telecom C-band. In contrast, waveguide-integrated SNSPDs achieve high absorption efficiencies without the need for optical trapping structures that rely on interference for enhancing the interaction of a single-photon with the nanowire. Instead, photons are absorbed along their direction of propagation in a traveling-wave geometry, employing a superconducting nanowire on top of a nanophotonic waveguide. Here, the interaction length can be engineered without imposing any bandwidth restrictions that would compromise the broadband material absorption capabilities. So far, however, waveguide-integrated SNSPDs have only yielded very limited system detection efficiencies and were restricted in bandwidth due to the limited capabilities of commonly employed fiber-to-chip interfaces,[8–10] e.g., grating couplers.

These restrictions can be overcome with 3D polymer coupling structures produced in direct laser writing (DLW).[11] Such 3D coupling structures achieve highly efficient interfaces with broadband performance by total internal reflection (TIR) and near-adiabatic conversion from optical fibers with large mode field diameter to nanophotonic waveguides with strong optical confinement.[12] Here, we show how combining such optical interfaces with state-of-the-art waveguide-integrated SNSPDs provides an efficient single-photon counting solution for the visible to infrared spectral region in a single device. The high system detection efficiencies, low dark count rate, and high timing accuracy our detectors achieve over the 500 nm–1650 nm wavelength range would, for example, allow for characterizing all single-photon sources under investigation with the same device. Rather than resorting to a wide range of radically differing counting solutions with varying performance, our broadband single-photon detector would, thus, allow for a one-to-one comparison of critical performance benchmarks for single-photon sources ranging from systems as diverse as lead vacancies in diamond (ZPL: 520 nm),[13] over other color centers in diamond (e.g., GeV, NV, SiV, and Sn), arsenide- and nitride-quantum dots, CdSe(Te)/ZnS- and PbS/CdS-quantum dots, defects in SiC, CNTs, defects in hBN and other TMDCs (e.g., WSe_2 and $MoSe_2$), G- and W-centers in silicon, rare earth emitters, single atoms, ions and molecules to implementations of spontaneous parametric downconversion, and spontaneous four-wave mixing sources reaching into the telecom C- and L-bands.[4,14–22]

Our device combines a U-shaped SNSPD on top of a Si_3N_4-waveguide that interfaces with an out-of-plane optical fiber via a 3D polymer coupling structure, as shown in Fig. 1(a). Optimal alignment between an optical fiber array and the device is achieved by optimizing the transmission through a neighboring reference coupling structure, as shown in Fig. 1(b). The 3D couplers collect the light incident from an optical fiber with a spherical lens, reflect it off a polymer-air interface slanted for total internal reflection, and near-adiabatically taper the mode field diameter down to the size of the Si_3N_4-waveguide. This coupling approach was previously shown to achieve efficient broadband transmission from 500 nm to 1650 nm.[11,12] Wide-band transparent Si_3N_4-waveguides then route light with negligible loss to the detector region, where waveguide-integrated SNSPDs fabricated from niobium titanium nitride (NbTiN) thin films allow for single-photon detection with internal quantum efficiencies consistent with unity.[23]

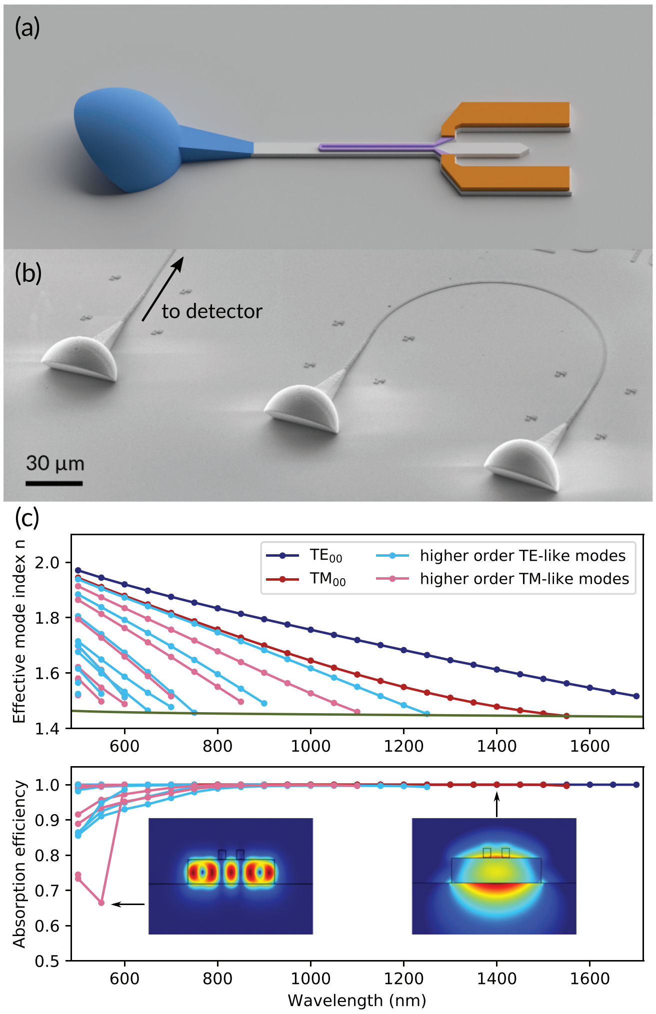

FIG. 1. (a) Illustration of a waveguide-integrated superconducting nanowire single-photon detector coupled to a wideband total internal reflection coupler. The U-shaped NbTiN nanowire (purple) is electronically accessible via radio frequency (RF) pads (gold) and placed on-top of the Si_3N_4 waveguide (white). Light can be coupled from a fiber array pending atop the total internal reflection coupler (blue). Both waveguide and TIR coupler are on-top of a SiO_2 substrate. In this design, light of different wavelength is reflected at the TIR plane of the coupler and adiabatically guided into the waveguide. The light then travels inside the waveguide and is absorbed by the nanowire atop. (b) Scanning electron micrograph of the power input coupler to the detector (left) and the two reference couplers (right) connected via a waveguide for optical alignment inside the cryostat. (c) FEM simulation of the effective refractive index n (top) of existing TE- and TM-like modes for different wavelength inside the waveguide, with an absorptive nanowire on top. The cutoff (green) is defined by the SiO_2 substrate. The resulting absorption efficiency (bottom) vs wavelength for a detector length of 150 μm shows near-unity absorption efficiency over a $>$1000 nm wavelength window.

The absorption efficiency, on the other hand, is dependent on photon wavelength, optical mode distribution inside the waveguide, and detector length. We perform 2D finite element method (FEM) simulations (COMSOL) for determining the wavelength dependence of the effective refractive index for the lowest transverse electric (TE) and transverse magnetic (TM) modes in a 1.2 μm wide and 330 nm high Si_3N_4-waveguide, as shown in Fig. 1(c) (see supplementary material for more details). Near-unity absorption efficiency is, thus, achievable for most modes when using a detector length of 150 μm, which, however, decreases when approaching wavelengths below 700 nm as more modes with varying field strength at the nanowire positions are allowed inside the waveguide.

We realize our waveguide-integrated SNSPDs using state-of-the-art thin film processing techniques in a top-down approach from a NbTiN/Si_3N_4/SiO_2-on-Si layer stack. Nanowires of 100 nm width are patterned in electron-beam lithography using HSQ resist and CF4-based reactive ion etching out of an approximately 4 nm thin NbTiN film that was deposited at room-temperature.[23] The waveguides are realized in a subsequent electron-beam lithography step employing AR-N resist as a mask during CHF_3/O_2 plasma etching. In a last fabrication step, we use 3D direct laser writing to produce the coupling structures using IP Dip (Nanoscribe) as a resist, which are precisely aligned to a tapered waveguide region using local reference markers for alignment.

The device is mounted inside a closed-cycle cryostat that allows for continuous operation at 1.4 K. We use a three-axis translation stage (attocube) inside the cryostat for bringing the chip into electrical contact with a radio frequency probe and aligning the device to an optical fiber array and optimize the transmission through the reference device [see Fig. 1(b)], as explained in previous work.[24]

We determine the system detection efficiency, SDE, for our devices by comparing the count rate recorded with the SNSPD, R, to the predetermined photon flux Φ_{in} inside the fiber going into the cryostat

$$\mathrm{SDE} = \frac{R - R_{dc}}{\Phi_{in}}.$$

R_{dc} here denotes the dark count rate, which we measure when blocking all input to the fiber guiding light to the device. In this way, the SDE includes all optical losses induced by both fiber and waveguide as well as misalignment between fiber and device or other coupling losses.

In order to test the detector over a broad wavelength range, we use several laser sources covering the 1461–1640 nm (Toptica CTL-1500 and Santec TSL-710) and 700–1000 nm (Spectra Physics Mai Tai HP) wavelength ranges, a diode pumped solid state laser at 532 nm (Laserglow), a HeNe-laser at 633 nm (Lasos), and diode lasers at 1055 nm, 1271 nm, 1300 nm, and 1393 nm. We use calibrated power sensor modules (HP 81530A for 533 nm–1000 nm and HP 81635A for 1055 nm–1640 nm) for determining the optical power at the input facet of the fiber and for monitoring the stability of the laser output. For the wavelength range of 900 nm–1640 nm, we use two optical attenuator units operated in series (2× HP 8156A) to obtain photon fluxes of 10^5–10^6 photons per second. For wavelength ranges where the optical attenuators (and intermediate fibers) cannot readily be assumed to operate in the single-mode regime anymore, we add appropriate single-mode fibers as mode filters between the attenuator units, thereby eliminating inter-dependence between the two units (see supplementary material for more details). Each SDE measurement is then obtained by manually switching fibers from the power sensor to the input fiber of the SNSPD and setting the attenuation levels for a desired photon flux. The input fiber to the SNSPDs that connects the outside of the cryostat to the detector is part of an optical fiber array consisting of standard telecom single-mode fibers. For the wavelength range below 900 nm, where no calibrated optical attenuators were available to us, we instead work with a higher input flux of up to 10^7 photons per second, which allows for calibration with the power meter set to the highest sensitivity range. We note that the high input photon flux leads to slightly underestimating the detection efficiency due to the dead time of the device. We further use polarization controllers for maximizing the recorded count rate because the SDE of our SNSPD is polarization dependent for some of the considered wavelengths.

In Fig. 2, we show the normalized count rate as a function of bias current supplied to the SNSPD. We determine the latching point of the detector at (15.2 ± 0.3) μA when no light is incident. We observe saturating count rates for all wavelengths between 532 nm and 1640 nm and find that the onset of saturation shifts to lower bias currents as the photon wavelength (energy) decreases (increases). In agreement with previous reports,[25] we observe that the bias current, at which the count rate reaches a given fraction of its maximum value, depends nonlinearly on the photon energy (Fig. 2, inset) and asymptotically approaches a minimal bias current value as the photon energy increases. The nature of this dependence is a matter of ongoing studies.[25–28]

The saturation behavior of the photon count rate further indicates that the detector can be operated in a bias current range <9 μA, where <25 dark counts per second are recorded, rising to 350 dark counts per second at 14 μA. While these are generally attracting performance characteristics, they particularly benefit the detection of photons with <1000 nm wavelength.

The overall SDE as a function of photon wavelength is shown in Fig. 3. We find a maximum SDE of (73 ± 5) % at 1271 nm, efficiencies above 58% for all wavelengths between 1055 nm and 1640 nm, and above 28% for all wavelengths between 633 nm and 1000 nm, which drops to (22 ± 6) % at 532 nm. The error bars of the SDE in Fig. 3 account for the uncertainty of the power meter, the attenuators, the laser stability, as well as statistical fluctuations over multiple measurements. We note that the measurement uncertainties are significantly larger at lower wavelengths, as increasing numbers of higher-order

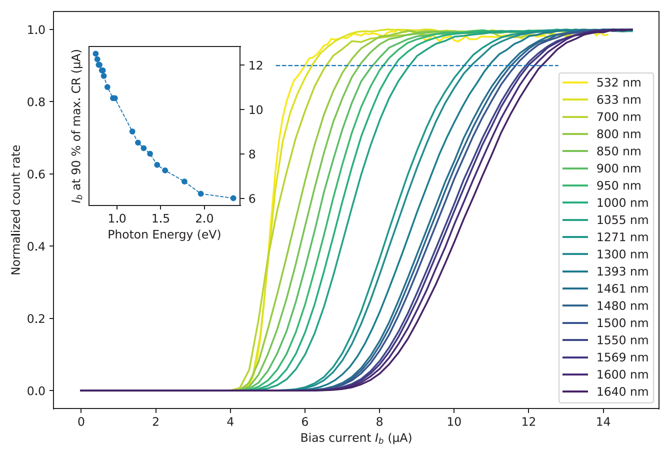

FIG. 2. Normalized count rate vs bias current. The onset of saturation of the count rate (and therewith also SDE) shifts to lower bias currents as the photon wavelength (energy) decreases (increases). Inset: bias current of the detector at 90% of the maximum count rate, indicated by the dashed line in the main figure.

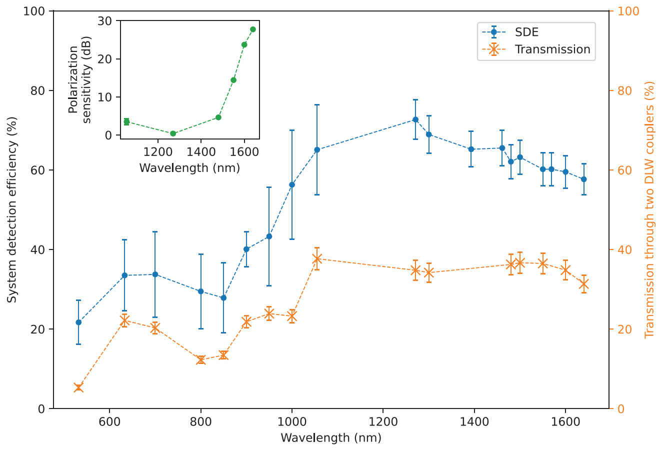

FIG. 3. Left axis: system detection efficiency dependence on photon wavelengths. The efficiency includes all losses from the input facet of the fiber going into the cryostat and was measured at bias currents where 98% of the respective maximal count rate is reached. Right axis: measured transmission through two 3D polymer couplers connected by a 180° bent waveguide. Inset: polarization dependence of the detector in the infrared range. The extinction ratio is measured by setting the count rates to their respective minimum and maximum values using a fiber polarization controller. Connecting lines are a guide for the eye.

modes in the fibers and photonic devices lead to larger calibration uncertainties of the attenuators, and the power sensors show larger uncertainties at the low input powers that were required for measurements of wavelengths shorter than 900 nm.

Wavelength-dependent variations of the SDE reflect the transmission characteristics of the fiber-to-chip interface and the dependency of the absorption efficiency in the nanowire on the optical field distribution in the waveguide. For the latter, we expect near-unity absorption of all photons with wavelengths greater than 900 nm in the 150 μm long SNSPD, where FEM simulations show that only the lowest TE and TM modes with significant field strength at the nanowire location need to be considered [see Fig. 1(c)]. At lower wavelengths, the absorption efficiency remains above 90% for most modes, which combines with near-unity internal quantum efficiency, as evident from the pronounced saturation behavior in the bias current dependence of the recorded detector count rates (see Fig. 2).[23] Consequently, and in agreement with previously reported high on-chip detection efficiencies,[10,23,24,29] we infer that the overall SDE is most strongly dependent on the transmission and alignment through the 3D fiber-to-waveguide coupler. We substantiate this in transmission measurements through a reference device comprising two 3D couplers connected by a short waveguide [see Fig. 1(b)]. The transmitted power, shown in Fig. 3 (right axis), qualitatively follows a similar behavior as the SDE data set over the considered wavelength range. We note that a direct comparison of both data sets is limited as the couplers can only be characterized in pairs, which requires an additional waveguide bend and leads to a higher sensitivity to fabrication variations as well as positional and rotational alignment of the fiber array relative to the chip. A comparison with stand-alone detector technologies as well as waveguide-integrated detectors that do not require resonant optical structures, as shown in Table I, highlights the benefits of our approach.[4,30]

TABLE I. Comparison of the system detection efficiency and coupling method in cavity-free waveguide-integrated SNSPDs.

System detection efficiency (peak) (%)	Coupling method	References
2.19 (1550 nm)	Grating coupler	10
4.3 (1550 nm)	Grating coupler	8
~10 (1550 nm)	Butt coupling	35
32 (~1530 nm–1565 nm)	Butt coupling	9
73 (1271 nm), 60 (1550 nm)	DLW coupler	This work

We further study the polarization dependence of the detector system, which we show for the 1055–1640 nm spectral range in Fig. 3 (inset). The extinction ratio for each wavelength is determined from the minimum and maximum count rates achievable through manipulation with a fiber polarization controller. We find 27.7 dB extinction at 1640 nm and 14.4 dB at 1550 nm wavelength, which reduces toward shorter wavelengths as higher order TE and TM modes are allowed inside the waveguide [see Fig. 1(c)].

To determine the timing properties of our detector, we use an oscilloscope for measuring the dynamic device response when detecting a 1550 nm photon. Figure 4(a) shows the average of 1k signal traces yielding a decay time (1/e value) of $\tau = 9.8$ ns from a fit to the data using a $ae^{-\tau/t}$ functional behavior. The decay time is closely related to the detector dead time,[31] thus indicating the feasibility of up to 100 MHz detection rates with our device. We further analyze the output signal traces in order to assess the jitter performance of our detector. Electronic contributions to the overall jitter can be calculated as[32]

$$j_{\mathrm{elec}} = \rho/s,$$

where ρ denotes the voltage noise and s is the slew rate (first derivative) of the output signal trace. We extract a slew rate of 0.68 mV/ps at the trigger level [see Fig. 4(a) inset] and 15.9 mV (FWHM) of voltage noise, resulting in an electronic jitter contribution of $j_{\mathrm{elec}} = 23.4$ ps. The overall jitter is measured using a start-stop measurement with a pulsed 1550 nm wavelength laser of 40 MHz repetition rate. The measured jitter for our detector is presented in Fig. 4(b). Here, we use a Gaussian distribution as a fit to the data to extract the jitter as $j_{\mathrm{meas}} = 25.7$ ps from the full width at half maximum. We note that the measured jitter value comprises contributions from the aforementioned electronic jitter j_{elec}, the intrinsic detector jitter j_{det}, and the reference jitter j_{ref} of the pulsed laser and detection system as

$$j_{\mathrm{meas}}{}^2 = j_{\mathrm{det}}{}^2 + j_{\mathrm{elec}}{}^2 + j_{\mathrm{ref}}{}^2.$$

We determined the jitter of the laser and detection system in a previous experiment to 1.5 ps.[23] This yields an overall intrinsic detector jitter of $j_{\mathrm{det}} = 10.5$ ps, which is comparable to literature values achieved with cryogenic amplifier systems.[33,34]

In conclusion, we present a single-photon detector system with high system detection efficiency over a broad wavelength range from 532 nm to 1640 nm. Our device leverages the material absorption capabilities of superconducting nanowires in traveling wave geometry by providing efficient fiber-to-waveguide interfaces realized as 3D polymer structures produced in direct laser writing. Together with

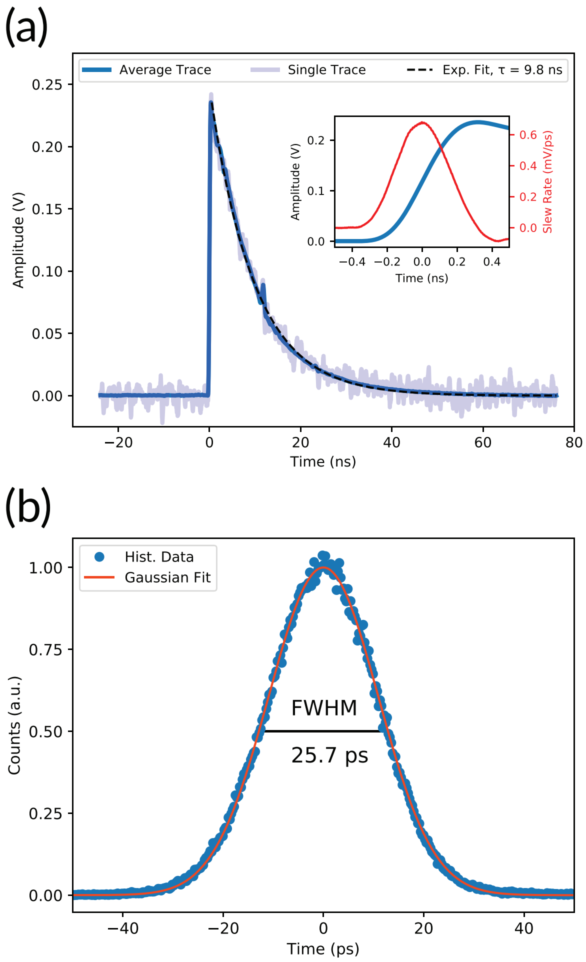

FIG. 4. (a) Dynamic timing response of the superconducting nanowire single-photon detector after the absorption of a 1550 nm wavelength photon. The decay time over an average of 1k traces (blue) yields a value of $\tau = 9.8$ ns extracted from an exponential fit. The FWHM noise on a single trace (blue) was determined to be 15.9 mV. Inset: zoom-in of the rise time of the detector, plotted with its first derivative, the slew rate. The slew rate (red) at the trigger level ($t = 0$) shows a value of 0.68 mV/ps. (b) Histogram data (blue) of the time difference of the arrival of a photon and the detection of the photon at the electrical readout (jitter). The measured jitter $j_{meas} = 25.7$ ps, extracted from the FWHM of a Gaussian fit (red), contains the jitter contributions of the electronic jitter, optical jitter, reference jitter, and the intrinsic jitter.

excellent timing resolution and small decay times, the architecture presented herein constitutes a major step toward the use of single-photon detectors in real-world applications such as the characterization of single-photon emitters, lifetime imaging, and quantum communication over a broad spectral range. Realizing attractive detector performance over such wide bandwidth will further benefit standardization efforts in single-photon counting.

See the supplementary material for details on simulation data, photon flux calibration, uncertainty estimation, and dark counts.

AUTHORS' CONTRIBUTIONS

M.A.W. and F.B. contributed equally to this work.

We would like to thank the Münster Nanofabrication Facility (MNF) for their support in nanofabrication-related matters. We acknowledge the support from the European Union's Horizon 2020 Research and Innovation Action under Grant Agreement No. 899824 (FET-OPEN and SURQUID). M.A.W. and J.S. acknowledge partial support by the Cells in Motion Interfaculty Centre. H.G. thanks the Studienstiftung des deutschen Volkes for financial support. C.S. acknowledges the support from the Ministry for Culture and Science of North Rhine-Westphalia (No. 421-8.03.03.02-130428).

DATA AVAILABILITY

The data that support the findings of this study are available from the corresponding authors upon reasonable request.

REFERENCES

[1]S. Pirandola, U. L. Andersen, L. Banchi, M. Berta, D. Bunandar, R. Colbeck, D. Englund, T. Gehring, C. Lupo, C. Ottaviani, J. L. Pereira, M. Razavi, J. Shamsul Shaari, M. Tomamichel, V. C. Usenko, G. Vallone, P. Villoresi, and P. Wallden, Adv. Opt. Photonics **12**, 1012 (2020).
[2]M. A. Taylor and W. P. Bowen, Phys. Rep. **615**, 1 (2016).
[3]F. Flamini, N. Spagnolo, and F. Sciarrino, Rep. Prog. Phys. **82**, 016001 (2019).
[4]M. D. Eisaman, J. Fan, A. Migdall, and S. V. Polyakov, Rev. Sci. Instrum. **82**, 071101 (2011).
[5]D. V. Reddy, R. R. Nerem, S. W. Nam, R. P. Mirin, and V. B. Verma, Optica **7**, 1649 (2020).
[6]A. Divochiy, M. Misiaszek, Y. Vakhtomin, P. Morozov, K. Smirnov, P. Zolotov, and P. Kolenderski, Opt. Lett. **43**, 6085 (2018).
[7]V. V. Vorobyov, A. Yu. Kazakov, V. V. Soshenko, A. A. Korneev, M. Y. Shalaginov, S. V. Bolshedvorskii, V. N. Sorokin, A. V. Divochiy, Y. B. Vakhtomin, K. V. Smirnov, B. M. Voronov, V. M. Shalaev, A. V. Akimov, and G. N. Goltsman, Opt. Mater. Express **7**, 513 (2017).
[8]C. Schuck, W. H. P. Pernice, X. Ma, and H. X. Tang, Appl. Phys. Lett. **102**, 191104 (2013).
[9]H. Shibata, T. Hiraki, T. Tsuchizawa, K. Yamada, Y. Tokura, and S. Matsuo, Supercond. Sci. Technol. **32**, 034001 (2019).
[10]W. H. P. Pernice, C. Schuck, O. Minaeva, M. Li, G. N. Goltsman, A. V. Sergienko, and H. X. Tang, Nat. Commun. **3**, 1325 (2012).
[11]H. Gehring, M. Blaicher, W. Hartmann, P. Varytis, K. Busch, M. Wegener, and W. H. P. Pernice, APL Photonics **4**, 010801 (2019).
[12]H. Gehring, A. Eich, C. Schuck, and W. H. P. Pernice, Opt. Lett. **44**, 5089 (2019).
[13]M. E. Trusheim, N. H. Wan, K. C. Chen, C. J. Ciccarino, J. Flick, R. Sundararaman, G. Malladi, E. Bersin, M. Walsh, B. Lienhard, H. Bakhru, P. Narang, and D. Englund, Phys. Rev. B **99**, 75430 (2019).
[14]M. W. Doherty, N. B. Manson, P. Delaney, F. Jelezko, J. Wrachtrup, and L. C. L. Hollenberg, Phys. Rep. **528**, 1 (2013).
[15]V. A. Norman, S. Majety, Z. Wang, W. H. Casey, N. Curro, and M. Radulaski, InfoMat **2020**, 1–24.
[16]P. Senellart, G. Solomon, and A. White, Nat. Nanotechnol. **12**, 1026 (2017).
[17]X. He, H. Htoon, S. K. Doorn, W. H. P. Pernice, F. Pyatkov, R. Krupke, A. Jeantet, Y. Chassagneux, and C. Voisin, Nat. Mater. **17**, 663 (2018).
[18]G. Moody, L. Chang, T. J. Steiner, and J. E. Bowers, AVS Quantum Sci. **2**, 041702 (2020).
[19]M. J. Holmes, M. Arita, and Y. Arakawa, Semicond. Sci. Technol. **34**, 033001 (2019).
[20]L. Caspani, C. Xiong, B. J. Eggleton, D. Bajoni, M. Liscidini, M. Galli, R. Morandotti, and D. J. Moss, Light: Sci. Appl. **6**, e17100 (2017).
[21]I. Aharonovich, D. Englund, and M. Toth, Nat. Photonics **10**, 631 (2016).
[22]S. Hepp, M. Jetter, S. L. Portalupi, and P. Michler, Adv. Quantum Technol. **2**, 1900020 (2019).

[23] M. A. Wolff, S. Vogel, L. Splitthoff, and C. Schuck, Sci. Rep. **10**, 17170 (2020).
[24] M. Häußler, M. Yu. Mikhailov, M. A. Wolff, and C. Schuck, APL Photonics **5**, 076106 (2020).
[25] M. Caloz, B. Korzh, N. Timoney, M. Weiss, S. Gariglio, R. J. Warburton, C. Schönenberger, J. Renema, H. Zbinden, and F. Bussières, Appl. Phys. Lett. **110**, 083106 (2017).
[26] D. Yu. Vodolazov, Phys. Rev. Appl. **7**, 034014 (2017).
[27] A. G. Kozorezov, C. Lambert, F. Marsili, M. J. Stevens, V. B. Verma, J. P. Allmaras, M. D. Shaw, R. P. Mirin, and S. W. Nam, Phys. Rev. B **96**, 054507 (2017).
[28] D. Yu. Vodolazov, Phys. Rev. B **90**, 54515 (2014).
[29] A. al Sayem, R. Cheng, S. Wang, and H. X. Tang, Appl. Phys. Lett. **116**, 151102 (2020).
[30] S. Ferrari, C. Schuck, and W. Pernice, Nanophotonics **7**, 1725 (2018).
[31] A. Vetter, S. Ferrari, P. Rath, R. Alaee, O. Kahl, V. Kovalyuk, S. Diewald, G. N. Goltsman, A. Korneev, C. Rockstuhl, and W. H. P. Pernice, Nano Lett. **16**, 7085 (2016).
[32] Q. Zhao, L. Zhang, T. Jia, L. Kang, W. Xu, J. Chen, and P. Wu, Appl. Phys. B **104**, 673 (2011).
[33] I. Esmaeil Zadeh, J. W. N. Los, R. B. M. Gourgues, V. Steinmetz, G. Bulgarini, S. M. Dobrovolskiy, V. Zwiller, and S. N. Dorenbos, APL Photonics **2**, 111301 (2017).
[34] I. Esmaeil Zadeh, J. W. N. Los, R. B. M. Gourgues, J. Chang, A. W. Elshaari, J. R. Zichi, Y. J. van Staaden, J. P. E. Swens, N. Kalhor, A. Guardiani, Y. Meng, K. Zou, S. Dobrovolskiy, A. W. Fognini, D. R. Schaart, D. Dalacu, P. J. Poole, M. E. Reimer, X. Hu, S. F. Pereira, V. Zwiller, and S. N. Dorenbos, ACS Photonics **7**, 1780 (2020).
[35] F. Najafi, J. Mower, N. C. Harris, F. Bellei, A. Dane, C. Lee, X. Hu, P. Kharel, F. Marsili, S. Assefa, K. K. Berggren, and D. Englund, Nat. Commun. **6**, 5873 (2015).